Neutronic design studies of a conceptual DCLL fusion reactor for a DEMO and a Commercial Power Plant

I. Palermo[1,2,*], G. Veredas[1,3], J.M. Gómez-Ros[1], J. Sanz[2], A. Ibarra[1]

[1]CIEMAT, Av. Complutense 40, E-28040 Madrid, Spain
[2]UNED, Dept. of Energy Engineering, c./ Juan del Rosal 12, E-28040 Madrid, Spain
[3]Max-Planck-Institut für Astronomie, Königstuhl 12, 69117 Heidelberg, Germany
*Corresponding author e-mail: **iole.palermo@ciemat.es**

Abstract
Neutronic analyses or, more widely, nuclear analyses have been performed for the development of a Dual-Coolant He/LiPb (DCLL) conceptual design reactor. A *detailed* 3D model has been examined and optimized. The design is based on the plasma parameters and functional materials of the Power Plant Conceptual Studies (PPCS) model C. The initial radial-build for the *detailed* model has been determined according to the dimensions established in a previous work on an equivalent *simplified* homogenised reactor model. For optimization purposes, the initial specifications established over the *simplified* model have been refined on the *detailed* 3D design, modifying material and dimension of Breeding Blanket, Shield and Vacuum Vessel in order to fulfil the priority requirements of a fusion reactor in terms of the fundamental neutronic responses. Tritium breeding ratio (TBR), energy multiplication factor, radiation limits in the TF coils, helium production and displacements per atom (dpa) have been calculated in order to demonstrate the functionality and viability of the reactor design in guaranteeing tritium self-sufficiency, power efficiency, plasma confinement, and re-weldability and structural integrity of the components. The paper describes the neutronic design improvements of the DCLL reactor, obtaining results for both, DEMO and Power Plant (PP) operational scenarios.

1. Introduction

Detailed neutronics analyses and realistic 3D models are required in order to generate the design specifications of a fusion demonstration reactor (DEMO) including breeding blanket (BB), shield and vacuum vessel (VV). A consistent neutronic optimization of structures between plasma and toroidal field (TF) coils is essential in the design work. The optimization process also involves the choice of materials, looking to guarantee the radiation limits on TF coils and structural components, preserving at the same time the tritium breeding capabilities and the power extraction performances of the blanket, trying to achieve the better compromise between these needs.

Starting from the radial build obtained in a previous work [1] on a *simplified* version of a Dual Coolant Lithium Lead (DCLL) DEMO reactor in which the structures were substitute by homogenised toroidal concentric layers, a new analysis has been performed on a more *detailed* one, focusing the design developments on the maintenance and improvement of the shielding efficiency and the tritium breeding capability.

From the beginning of the DCLL concept in 1994 [2] numerous designs have been developed around the world trying to achieve the best performances for a fusion reactor based on this concept. Different features have been applied for reaching them, such as the SiC flow channel inserts concept which was proposed for the first time in 1997 [3]. Following these early applications, the DCLL blanket concept has been used in power plant studies in Europe [4], China [5][6], and in the US [7], and became a base concept for the development of ITER Test Blanket Modules (TBM) in the US [8][9] and China [10][11]. USA have continued studying and developing many aspects of the DCLL concept especially for ARIES and ITER [12] while Europe, after the EU model C of the Power Plant Conceptual Studies (PPCS) of 2003 [13][14], has not dedicated further efforts to the improvement of this concept.

Since 2009, following the approaches proposed in the EU model C of the PPCS, the Spanish government has funded a research programme, called CONSOLIDER TECNO_FUS [15][16], for the development of a DCLL DEMO design and its Plant auxiliary systems. In this Programme, the neutronic activities have been focused on the optimization required to improve the performances of the design, in terms of tritium breeding ratio

(TBR), energy multiplication factor, shielding and radiation damage. The neutronic results of the explored modifications corresponding to the *detailed* 3D model are explained, analysed and summarised in this paper.

2. Key design features of the DCLL design

The dual-coolant blanket concept (figure 1) is mainly characterised by the use of self-cooled breeding zones with the liquid metal LiPb serving as a breeder for tritium and as a coolant for removing the heat gained from fusion energy. Its outlet temperature has to be maximised for efficiency reasons. In this design, corresponding to an high temperature DCLL concept, the liquid metal enters the modules at 480 ºC and leaves them at 750 ºC, which is above the maximum permissible temperature for steel. Therefore, the LiPb channels have to be thermally insulated with a 5 mm thick layer of SiC_f/SiC flow channel inserts (FCIs) serving as thermal insulators for the LiPb channels that minimise pressure losses and allow for a relatively high LiPb exit temperature, leading to a high thermal efficiency, and as electric insulators (for MHD reasons). For the structure, a helium-cooled ferritic steel is used. High-pressure (8 MPa) helium gas is used to cool the first wall (FW) and the entire steel structure. The helium cooling circuit (figure 2) has been ideated to parallelize the flow to the maximum, avoiding unnecessary collectors. The first wall and the inner crosshead are part of a single continuous path, single-run, with no internal manifolds. The inlet temperature of the helium amounts to 320 ºC, the outlet temperature to 525 ºC; the helium at lower temperature goes to the first wall and countercurrent flows are created to stabilize thermal gradients minimising the thermal stresses.

Instead of "large modules", like in the PPCS' model C, the design here analysed uses "banana-shape" segments to facilitate a faster remote maintenance in order to guarantee higher availability of the reactor. Each single module has a total channel length of ~21m. The module is comprised of 150 plates with inner He channels. Each banana module consists of 4 LiPb channels, 2 for the inlet and 2 for the outlet of the liquid metal. The LiPb inlet and outlet are in top and LiPb enters to the first wall (figure 1). The LiPb channels have round corners for a better flow, and the flow velocity is 0.15 m/s. The Shield is acting also as distributor and collector of the helium channels, having the dual task of He entry and exit (figure 2). The Shield specific part is 15 cm thick, and the Collector function occupies other 15 cm.
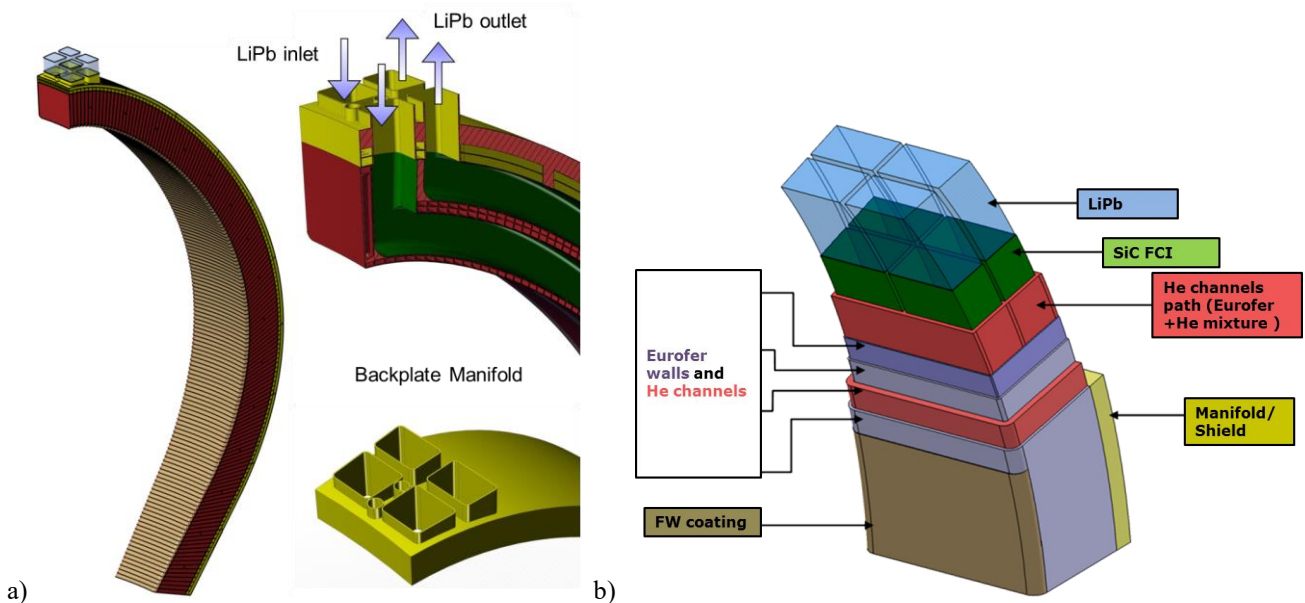
Figure 1. "Banana-shaped" breeding blanket module composed by four LiPb channels, two for the inlet and two for the outlet of the liquid metal. The LiPb inlet and outlet are in top (a); scheme of the breeding blanket's internal structures (b).
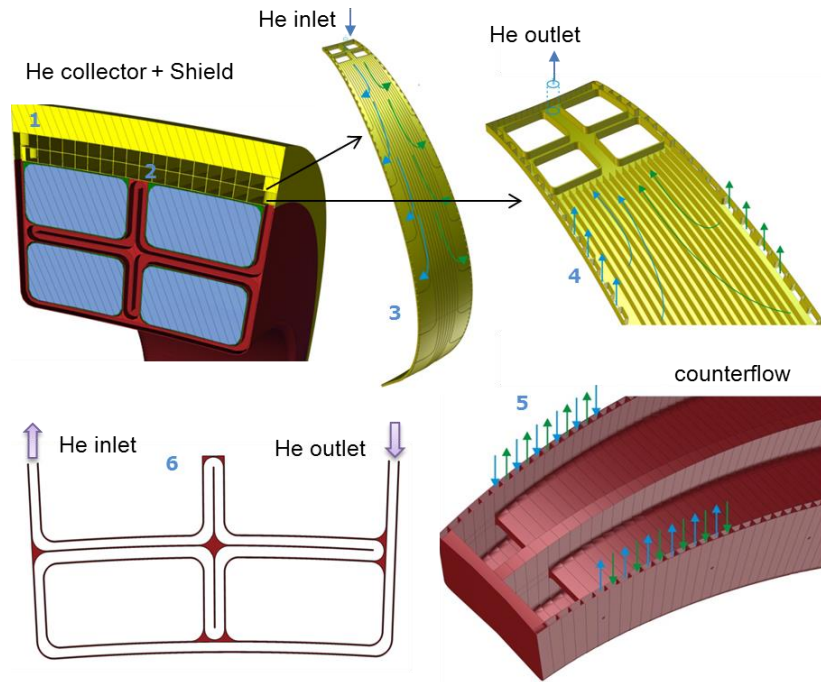
Figure 2. Cooling cycle: the shielding function (1) and the manifold (2) are separated in the CAD model although the neutronic model considers an equivalent mixed material composition for the entire thickness. The Manifold operates as distributer of the inlet helium (outermost layer, 3) as well as collector of the outlet helium (innermost layer, 4). The inlet channels distribute the helium at different heights (3: green and blue arrows) of the walls of the blanket and there enter in countercurrent (5: in one channel the helium enters from the right and exits from the left and, in the next channel just below, the helium enters from the left and exits from the right). Inside the blanket (6) the helium passes through the side wall, the first wall, half of the opposite side wall, the inside crosshead and exits by the other half of the side wall, continuously. The helium is finally collected at different heights (4: Blue and green arrows) by channels located in the lower layer of the Manifold.

3. Modelling and calculation procedure

3.1 Neutronic model

Realistic 3D models are required for accurate calculations, particularly in order to avoid the overestimation of tritium breeding ratio [17] and nuclear heating values in in the first wall and front zone of the blanket, as well as the underestimation of the radiation damage and nuclear heating at the back [18], when 1D models are used. The model considered in this work is the *detailed* 3D version of a previously simplified DCLL [1]. Thus, the TF-coils, the divertor, the BB helium channels, the SiC flow channel inserts, the "banana-shape" breeder modules, the Vacuum Vessel and the Upper Port are now realistically modelled in order to determine the influence of accurate 3D modelling on the neutronic performance.

The reactor consists of 12 sectors of 30º (figure 3a and figure 4a), each of one equipped with an Upper Port for the Remote Handling operations and hosting the connexions to the auxiliary systems. Each 30º sector is then composed by 2 inboard (IB) blanket banana segments of 15º and 3 outboard (OB) segments of 10º for a total of 60 blanket modules. For neutronics purposes, a single 30º sector has been studied taking advantage of the toroidal symmetry of the tokamaks. The neutronic design (figure 3b) has been created by means of a software specifically developed to replace the irregular profiles of the CAD model (splines and curves based on equations that generate surfaces of an order higher than the admitted by the Monte Carlo transport code) by the union of segments that approximate the profile within a tolerance value pre-established by the user (distance of the chord to the curve). The program also allows the user to choose some basic parameters for the plasma and the reactor components.
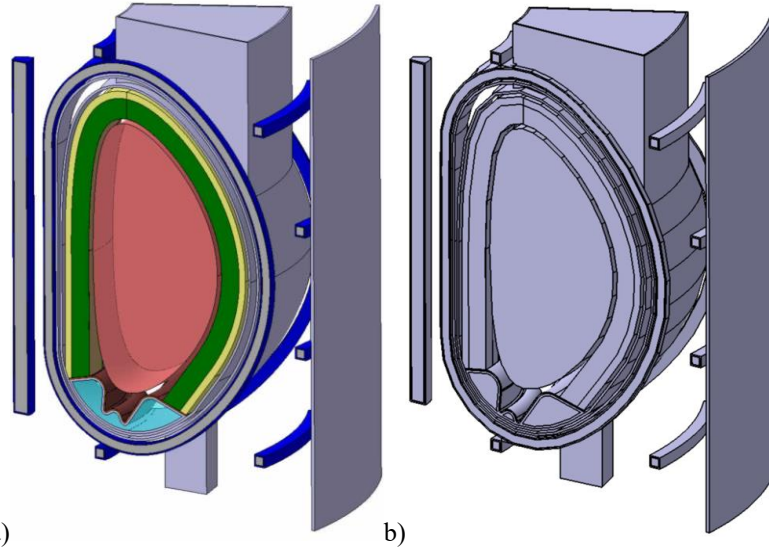
Figure 3. 30º sector of the original *detailed* 3D CAD (a); 30º sector resulting from the approximation, that now can be used by the transport code (b).

In the horizontal cross section at the mid plane represented in figure 4, the radial coordinates for all the components of the IB (b) and OB (d) sides are given. IB and OB BB are symmetric and their thickness from the FW to the Shield is 1.15 m. On the contrary, the VV thickness, along the D-plasma profile, is not constant (see table 2) and varies from the IB to the OB. The circle of figure 4c gives details of the breeder zone components (first wall, helium channels and SiC flow channel inserts).
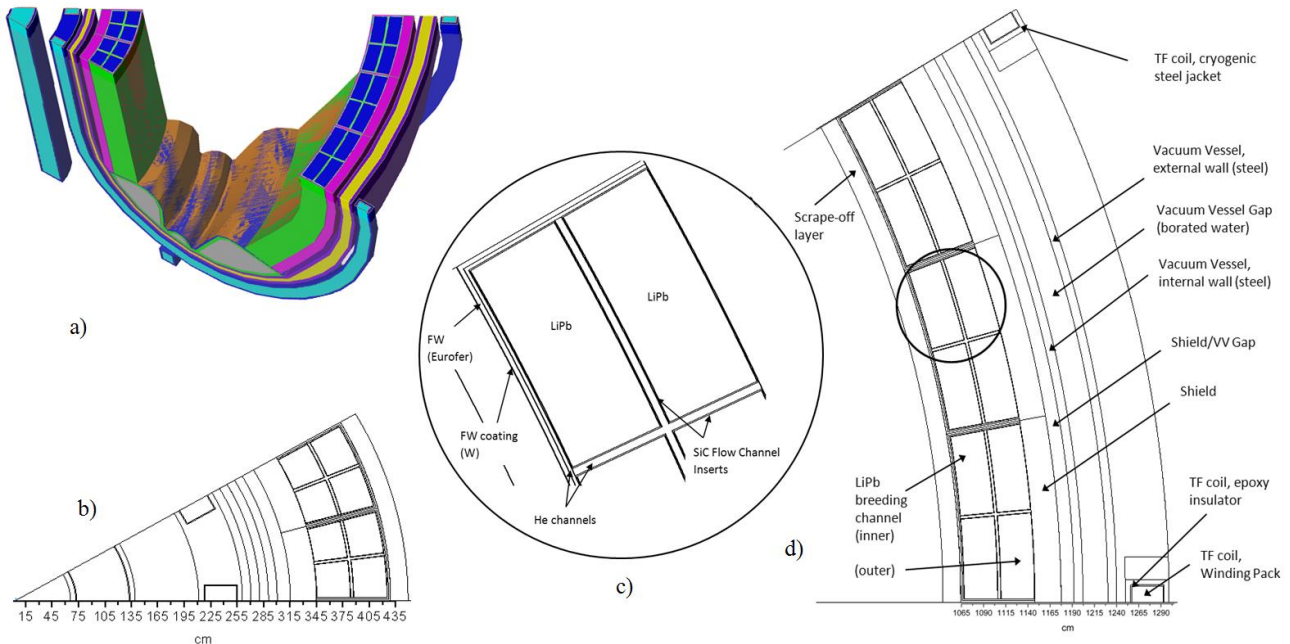
Figure 4. Cut of the 30º sector of the *detailed* DCLL design (a) and horizontal cross-section with radial coordinates (in cm) of the IB (b) and OB (d) sides and names of each constituent. In the circle (c), the inner structures of the blanket.

After the simplification that maintains unaltered the fundamental constituents of the reactor design, the STEP model is completed by means of the MCAM interface program [19] with the needed voids cells in order to fill all the space in which the particle transport has to be kept. Then, the model is converted by MCAM into the geometric input of the Monte Carlo code MCNPX [20]. The minor conversions errors are then fixed up to reduce the number of lost particles during the transport, and thus the model can be used for the transport analysis.

3.2 Materials

In modelling all the fundamental components, the heterogeneities have been taken into account realistically by associating the corresponding materials. A realistic composition for the LiPb has been considered [21], with 9.6 gr/cm^3 density, 90% Li-6 enrichment and with eutectic point at 15.7 [22]. The structural materials are mainly ferritic–martensitic steel Eurofer-97 in the BB and Shield, and austenitic steel 316-LN in the VV. The double wall vacuum vessel consists of 100 mm thick SS-316L walls, filled with variable thickness of borated water. Boron content in the borated water is 1.32 wt% at 40 °C, the concentration ratio of ^{10}B in boron is enriched up to 95% in order to improve the neutron shielding performance [23][24]. However, the helium channels in the Shield as well as the water cooling channels in the Vacuum Vessel interior space are not modelled, so mixed materials compositions (water or helium + steel) have been used for the two systems. Otherwise the TF coil is now realistically designed being made by an external steel jacket (6 cm thick), an epoxy insulator (1 cm thick) and an internal mixture that represents the winding pack (WP) (36 cm^2) for a total of a 50 cm^2 section. Thanks to this improvement in the neutronic design it will be possible to assess specific neutronic responses on these three main TF coil components, as will be presented in the next sections. Since a divertor design has not been already developed, the 3D *detailed* model takes a conservative assumption by including water-cooled steel (Eurofer 97) with 10 mm tungsten first wall and 50 mm copper second wall. The compositions for all the components are summarised in table 1.

Table 1. Composition of the reactor components for the initial *detailed* model.

Component		Material or Composition of the mixture in vol %				
		Other	Eurofer	He	SS316LN	H$_2$O
Breeding Blanket	First Wall coating	W				
	First Wall		100			
	Helium channels		38.5	61.5		
	Flow channels inserts	SiC				
	Breeder zone	LiPb				
Shield			65.93	34.07		
Vacuum Vessel	Inner wall				96.5	3.5
	Filler	B (0.52)			4.18	95.3
	Outer wall				95.3	4.7
TF coil	Casing				cryogenic	
	Insulator	epoxy-glass				
	Winding Pack	Nb$_3$Sn (2.895), Cu (11.69), Bronze (7.35), r-epoxy (18), void (0.055)		16.82 (liq.)	43.19	
Cryostat					100	
Divertor	First wall	W				
	Second wall		100			
	Third wall	Cu				
	Coolant					100

3.4 Radial Build

In the previously published work [1], although the shielding optimization was not completely achieved, it was noted that an enlargement of the Eurofer First Wall thickness could improve the global shielding performance of the design with no invalidating impact on the tritium breeding performance of the blanket. In fact, by adding 2 cm of Eurofer to the initial 1 cm of Eurofer thickness (total 3 cm of Eurofer) it was reduced the radiation at the TF coil, keeping the Tritium Breeding Ratio (TBR) higher (being 1.18) than the threshold (1.1) needed for the reactor fuel self-sufficiency [25]. In the new *detailed* model, as the tritium production could be reduced due to the presence of structure's details, a prudent option of 2 cm for the Eurofer FW has been considered together with a more risky one of 5 cm. The radial build of the BB + Shield in the 2 cases is summarised in table 2.

Table 2. Thicknesses of the BB and Shield components in the two different cases here analysed for the *detailed* first version of the model (IB and OB sides have the same thickness).

Component	thickness (mm)		Total thickness (mm)	
	Case1	Case2	Case1	Case2
First Wall coating (W)	0.01	1	-	-
First Wall (Eurofer)	50	19	0.01	1
Helium channels	15	15	50.01	20
Flow channels inserts (SiC)	5	5	65.01	35
Breeder zone (LiPb)	370	385	70.01	40
Flow channels inserts (SiC)	5	5	440.01	425
Helium crosshead channel	30	30	445.01	430
Flow channels inserts (SiC)	5	5	475.01	460
Breeder zone (LiPb)	370	385	480.01	465
Flow channels inserts (SiC)	5	5	850.01	850
Shield (Eurofer)	300	300	855.01	855
TOTAL			1155.01	1155

3.3 Plasma parameters

The nuclear calculations have been carried out for a 3450MW fusion power equivalent to a source term of 1.23×10^{21} n/s . The same plasma specifications as those of the PPCS model C [13] have been assumed as reference (table 3). An external FORTRAN90 source subroutine has been developed [26] for sampling the position of the emitted neutrons according to the neutron source density distribution in a tokamak.

Table 3. Main plasma parameters used as reference.

Model C parameters	value
major plasma radius	7.50 m
minor plasma radius	3.00 m
elongation	1.9
triangularity	0.47
peak factor	1.7
radial shift	0

Once established the geometry, the materials compositions and the source term, the neutronic analyses have been performed using the Monte Carlo code MCNPX 2.6 [20] and cross section data ENDF/B-VII [27] and MCLIB04 [28] to simulate the coupled neutron/photon transport. Intensive use of the CIEMAT supercomputing cluster EULER has been required as well as variance reduction techniques to achieve low enough statistical uncertainties.

As inherent to the plasma characteristics, the neutron wall loading (NWL) has been firstly assessed as distribution in the inboard (IB) and outboard (OB) poloidal regions of the plasma surface depicted in figure 5a. The peak NWL values have resulted 2.12 and 2.71 MW/m^2 for the IB and OB sections, respectively. The entire poloidal variation of the NWL is presented in figure 5b where the average value of 2.21 MW/m^2 is also shown.
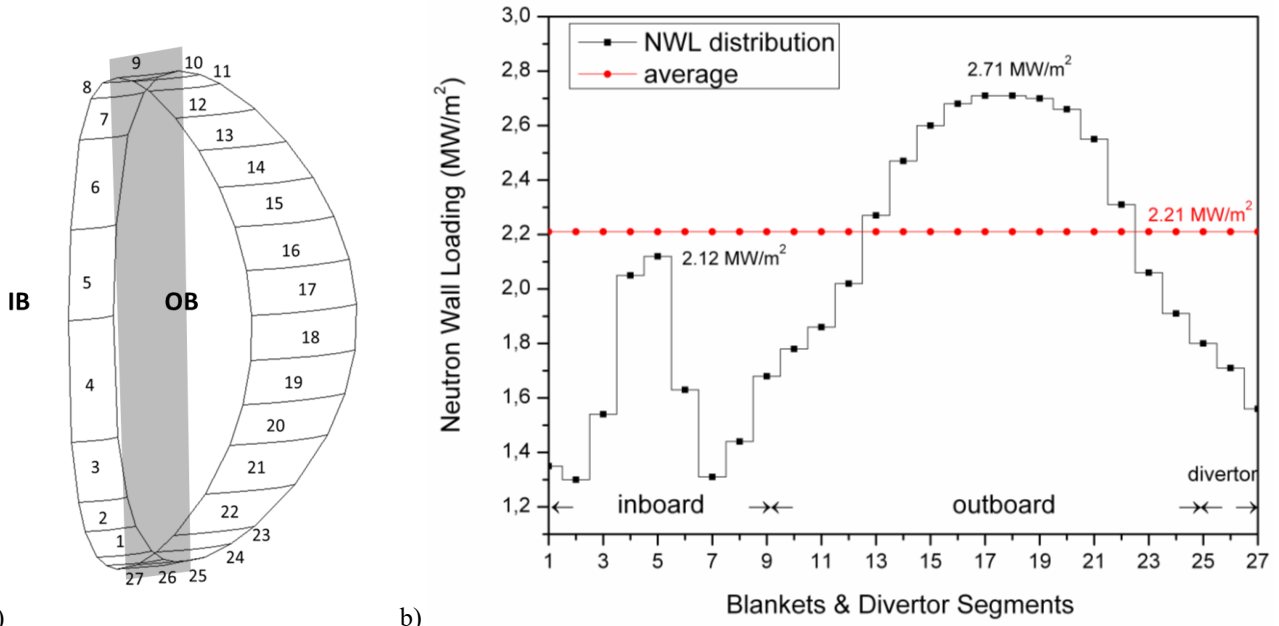
Figure 5. Poloidal zones in which the NWL has been calculated (a); NWL average value and NWL poloidal distribution in both IB and OB segments and in those which correspond to the divertor (b).

4. Optimization and Results

4.1 Neutronic analysis of the initial design

The comparison between the two *detailed* options (with 2 cm and 5 cm of Eurofer FW) and the similar old *simplified* version [1] is shown in the table 4 in which the basic responses Tritium Breeding Ratio (TBR), Peak Nuclear Heating (PNH) and Energy Multiplication (M_E) factor are stated. The comparison, also concerning two different Li enrichments (50% and 90% in Li-6) and a pure vs. a realistic industrial LiPb composition [21], shows that 5 cm for the FW disables reaching the tritium breeding threshold (1.1). On the contrary, the 2 cm FW option allows ensuring tritium breeding self-sufficiency with a considerable margin (1.22) that will enable further developments in the model. Thus, the 2 cm FW option was chosen to perform further analysis.

Table 4. Comparison between the optimised version of the *simplified* model [1] and the similar *detailed* versions. Two thicknesses for the FW and its coating have been tested trying also two Li-6 enrichments and an ideal and a realistic industrial LiPb compositions. Fundamental neutronic results are reported.

model	Vacuum Vessel (mm)				First Wall (cm)	Li-6 % enrich.	TBR*		PNH** (W/m³)	M_E***
	W	VV Int	Filler	VV Ext			LiPb (no impurities) 10 gr/cm³	LiPb (realistic) 9,6 gr/cm³		
simplified	10	100	200	100	0,1 W 3 Eurofer	90%	1.18	-	1.76x10³	1.15
detailed	-	100	Variable: 100 *(IB)* 270 *(OB)* 440 (*top IB*)	100	0,01 W 5 Eurofer	50%	0.986	-	-	-
						90%	1.084	1.053	-	-
					0,1 W 2 Eurofer	50%	-	1.145	-	-
						90%	-	1.225	1.7x10⁴	1.141

*Tritium Breeding Ratio, **Peak nuclear heating in TF coils, ***Energy Multiplication factor*

Detailed distributions of tritium related parameters have also been studied for this configuration. Poloidal distributions of the tritium production (in atoms of tritium per fusion neutron source, at T/n) and of the tritium production rate density (at T/cm³ s) are given in figure 6. The last one, normalized to the volume of each zone, gives information about the efficiency of each poloidal region, useful if the banana-shape blanket system

would evolve to a modular blanket system in which each module could have a different thickness to make the most of its efficiency.
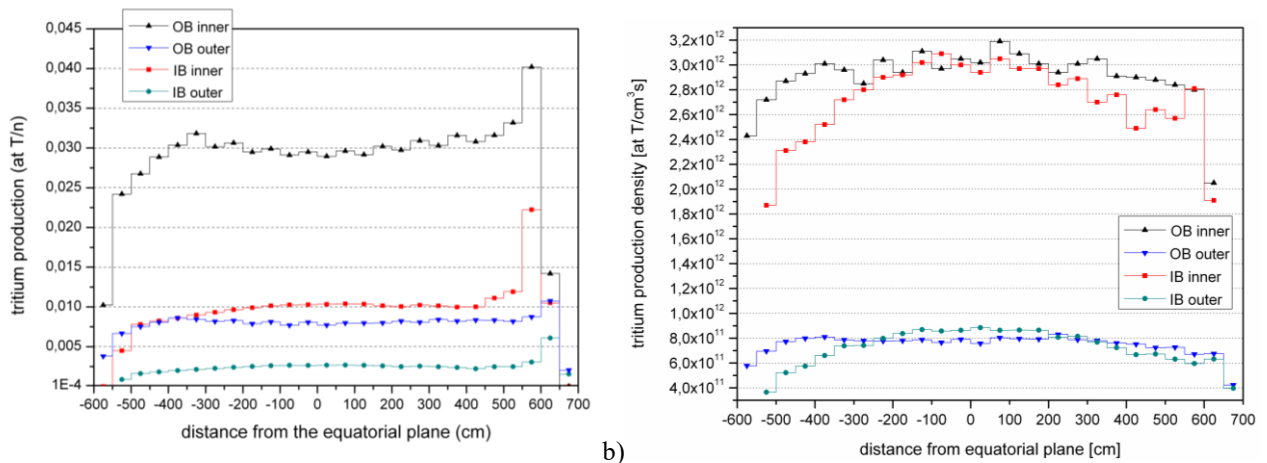
Figure 6. Poloidal distributions of the tritium production (at T/n) (a) and (b) of the tritium production rate density (at T/cm^3 s). Inner/Outer channels represent the closer/farther channels from the plasma.

For this option the energy multiplication factor M_E and the peak nuclear heating in the TF coil have been also calculated in order to verify that other fundamental requirements are kept. The M_E factor for this version is 1.14 taking into account that the power generated by neutrons and gamma in the whole reactor is 3150 MW. The radial distribution of the power density in the different components of the reactor is shown in figure 7, and maps distributions at the equatorial plane in the IB and OB side, from the FW to the TF-coil, are shown in figure 8. The maps give evidence of the streaming effect produced by the helium channels inside the blanket, and in the interface between blankets segments.
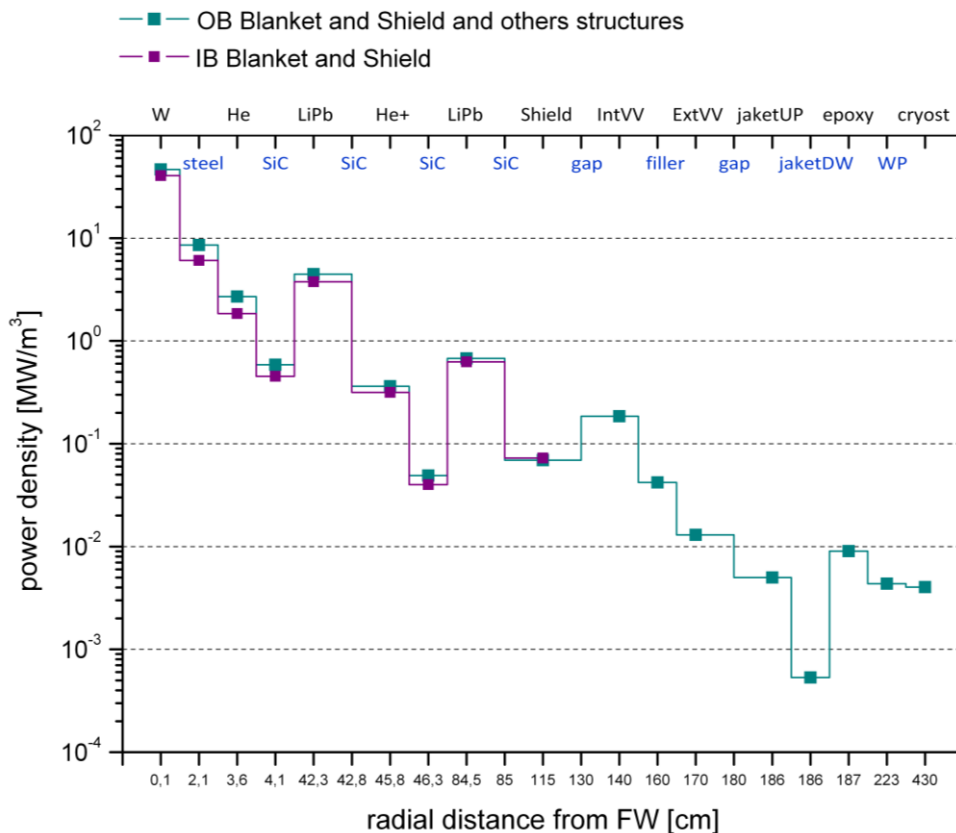
Figure 7. Radial distribution of the power density in the reactor's components.
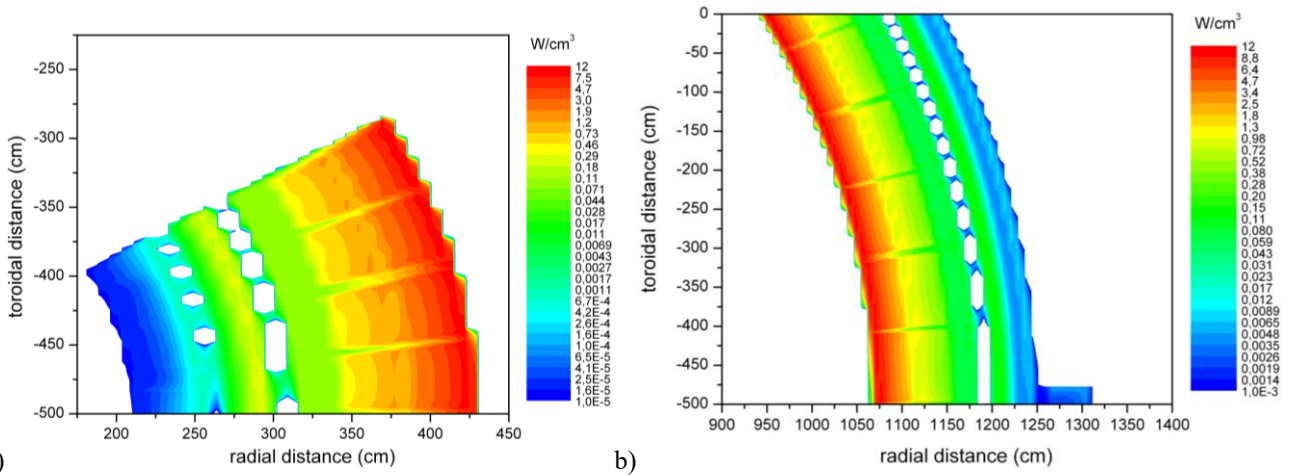
Figure 8. Power density radial-toroidal maps in the equatorial zone (between the planes at 10 and 60 cm from Z=0) in the IB (a) and OB (b) side of the 30º sector, from the FW to the TF-coil.

Regarding the nuclear heating in TF coil, table 4 shows that the peak results above the limit of 5×10^3 W/m^3 for the magnet *quench* [29]. The poloidal distribution of the power generated in the TF coil winding pack at different distances from z=0 is represented in figure 9a where the IB and OB side of the coil are separately depicted (blue and black lines, respectively). The figure gives evidence that the peak nuclear heating in TF coil exceed the limit of 5×10^3 W/m^3 (black dotted line) in the zone of the TF coil right behind the Upper Port of the VV (from 3 to 8 m high, approximately). This happens because the Port acts as an open duct for the emitted radiation which is poorly shielded and pass almost unattenuated through it, thus depositing its energy on the coil. The MCNP "mesh tally" (figure 9b) of the power density near the Port makes evident this behaviour.
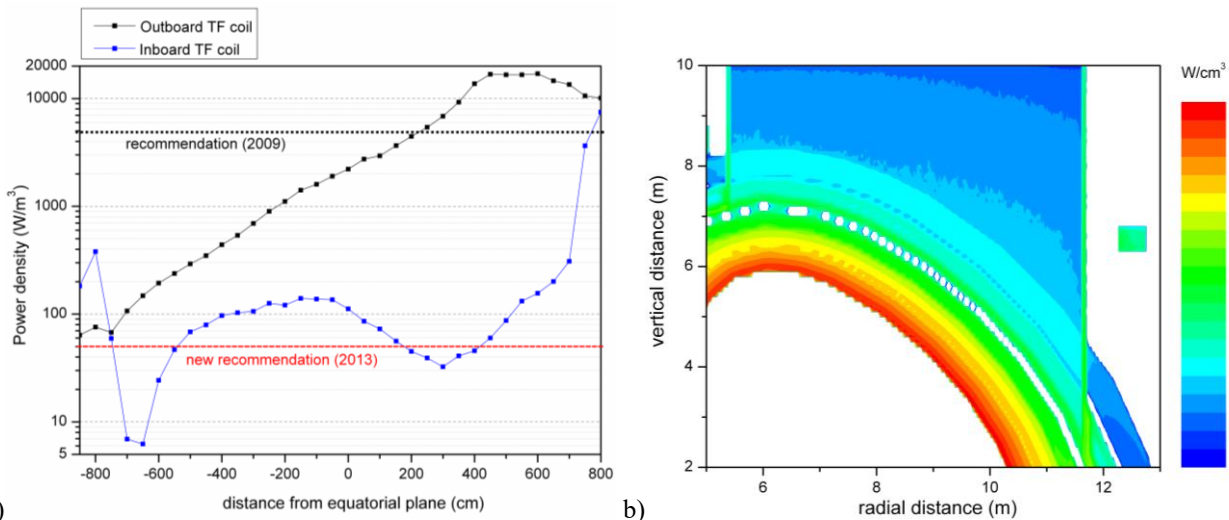
Figure 9. (a) Poloidal distribution of the power density (W/m^3) in the TF coil; (b) detailed radial-poloidal map distribution (W/cm^3) in the regions near the Upper Port showing the very high values (cyan) in the TF coil at that height.

During 2013 new recommendations [30] for the radiation limits at the TF coils have been established in the frame of the European activities towards DEMO design, as resumed in table 5, resulting, among others, in a reduction of the limit for the nuclear heating of two orders of magnitude from the previous one (being now 0.05×10^3 W/m^3) which has meant a reconsideration of the shielding systems developed until the moment in our designs. Indeed from figure 9a it is possible to see that almost at all heights of the TF coil the new limit (red line) is not fulfilled. It is worth mentioning that very high values occur in the coil region at divertor level, but the design of this component was out of the scope of this work.

9

Table 5. Radiation design limits for the superconducting TF-Coils. Comparison between the older [29] and the new [30] specifications showing that the nuclear heating limit have changed of two orders of magnitude.

Parameter	2009	2013
Integral neutron fluence for epoxy insulator [m^{-2}]	$\leq$2-3$\times10^{22}$	$\leq$1$\times10^{22}$
Peak fast neutron fluence (E>0,1 MeV) to the Nb_3Sn superconductor [m^{-2}]	$\leq$1$\times10^{22}$	
Peak displacement damage to copper stabiliser, or maximum neutron fluence, between TFC warm-ups [m^{-2}]	$\leq$1~2$\times10^{21}$ Equivalent to 0.5~1$\times10^{-4}$ dpa	
Peak nuclear heating in winding pack [W/m^3]	**$\leq$5$\times10^3$**	**$\leq$0.05$\times10^3$**

4.2 Vacuum Vessel and Upper Port modifications. Resultant nuclear heating in winding pack.

Due to the considerations just explained, in order to improve the shielding capability of the Vacuum Vessel walls and Upper Port, different approaches have been tested modifying materials compositions and components thicknesses of the original model according to the description summarized in table 6. The results in terms of power density in the TF coil provided by these modifications are presented in figures 10 a) (outboard) and b) (inboard). The first modification (model 2) has implied the use of 2 cm of tungsten (W) before the inner wall of the Vacuum Vessel (VV) as it was done in some of our previous *simplified* versions of the DCLL design [1]. Furthermore, the Port wall has been enlarged (from 10 to 30 cm) in order to be comparable at least with the VV walls thickness. In the second modification (model 3) tungsten carbide (WC) has been tested instead of pure tungsten. The choice of this material, already proposed in others DCLL studies [31][32], comes from the consideration that WC combines the neutron moderation provided by carbon with the neutron absorption and photons attenuation provided by tungsten. The two models (2 and 3) present very similar results (figure 10, red and blue lines) of the nuclear heating in the TF coil winding pack (WP) due to the fact that the gamma component is the highest contribution. In the next step (model 4) a 30% of W has been added to the inner and outer wall of the VV and to the Upper Port wall resulting in a remarkable improvement of the behaviour against radiation at all TF coil heights (dark cyan lines of figures 10).

Table 6. Summary of the configurations (materials and thicknesses) tested for the Vacuum Vessel. Compositions are given in volume %.

model	Gap Shield/VV	VV inner wall	VV Filler	VV outer wall	Upper Port
1	15 cm void	96.5% SS316LN 3.5% water	95.3% water 0.52% Boron 4.18% SS316LN	95.3% SS316LN 4.7% water	10 cm SS316LN
2	13 cm void 2 cm W	" "	" "	" "	30 cm SS316LN
3	13 cm void 2 cm WC	" "	" "	" "	" "
4	" "	66.5% SS316LN 30% W 3.5% water	" "	66.5% SS316LN 30% W 3.5% water	30 cm 66.5% SS316LN 30% W 3.5% water
5	Double Wall Upper Port: **10 cm** 66.5% SS316LN / 30% W / 3.5% water + **20 cm** 95.3% SS316LN / 4.7% water. + **horizontal shield**: 60% borated steel at 2% (ASTM-A887-89) + 40% water				
6	Double Wall Upper Port: **10 cm** 66.5% SS316LN / 30% W / 3.5% water + **20 cm** WC. + **horizontal shield**: 30% WC / 37.46% SS316LN / 31.46% water / 1.08% Boron				
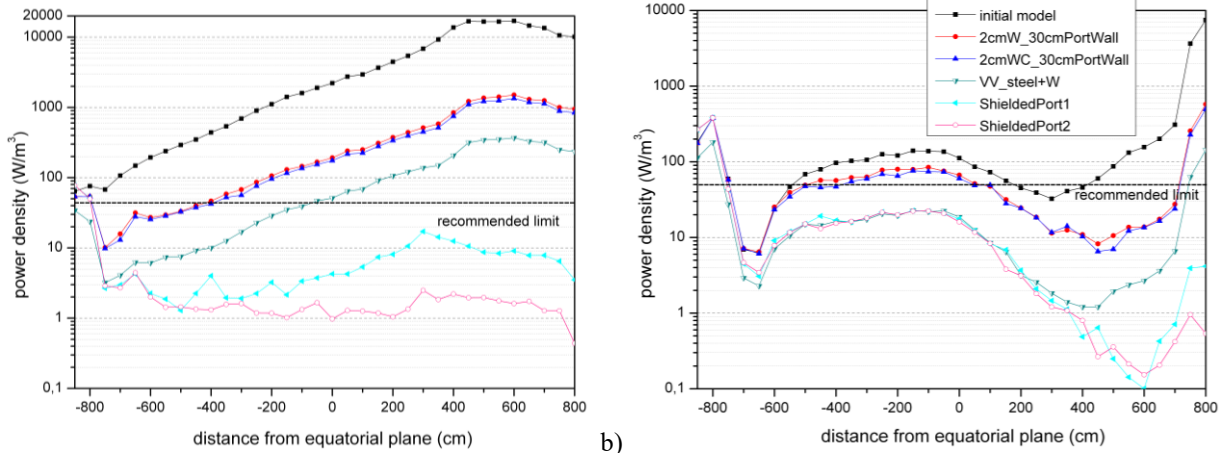
a)

b)

Figure 10. Poloidal distribution of the power density (W/m^3) in the OB (a) and IB side (b) of the TF coil WP for the different configurations of the VV.

Despite all, it was observed that the modifications were not enough to reduce the power density in the TF coil below the new limits, becoming evident the need of a more effective shield for the Upper Port. Thus, in models 5 and 6 an horizontal shield inside the Upper Port has been added similarly to the work made in [33]. Furthermore, the single Port wall of 30 cm has been substitute by 2 walls of 10 and 20 cm. In figure 11 are presented the previous Port, the double wall Port and the horizontal shield. In model 5 (that in the figure 10 is called "ShieldedPort1") an horizontal shield of borated steel and water has been used in a proportion of 6 to 4, that resulted the best choice in [33]. For model 6 ("ShieldedPort2") a mixture of borated steel, water and tungsten carbide has been tested (table 6). The results show a very good behaviour for both choices of shielded Ports (cyan and pink lines in figure 10) being the power density values under the recommended limit (except behind the divertor that was not object of study).
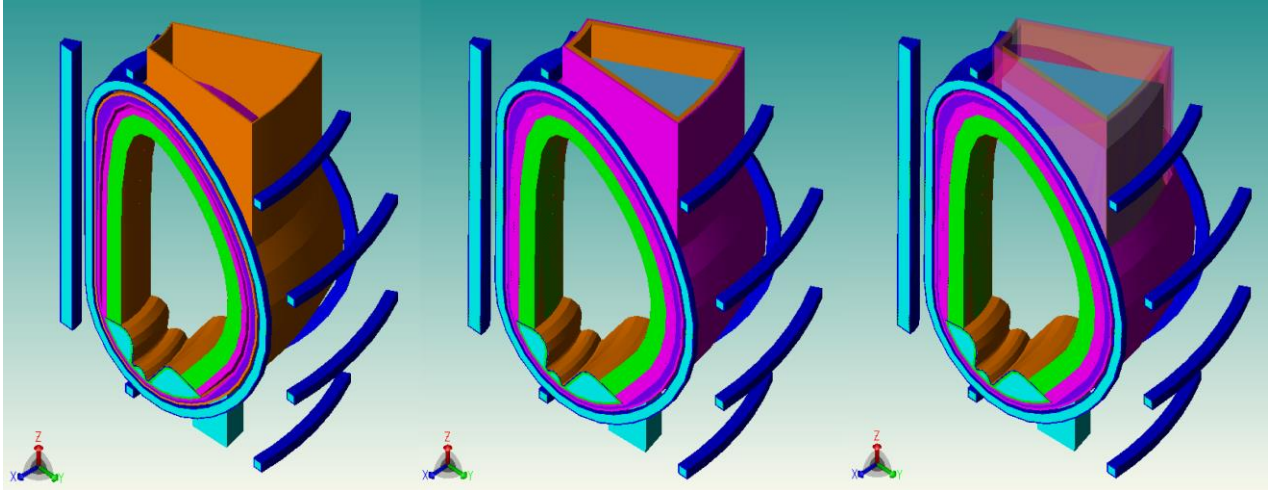
Figure 11. Optimization of the Upper Port: the single wall (left) is modified into a double wall (middle): the external (pink) is a 10 cm wall of W and steel, the internal (orange) is a 20 cm wall of steel or WC; (right) inside the walls, the Port is closed by an horizontal shield (cyan) that protects the Coils and the VV near there. Two compositions (described in table 6) for the horizontal shield have been tested.

A comparison in terms of power density (W/cm^3) of the two system with respect to the unshielded Port is shown in the maps of figure 12. The horizontal shield would solve also the necessity to protect the connexions to the auxiliary systems that are located in that zone [34].

11
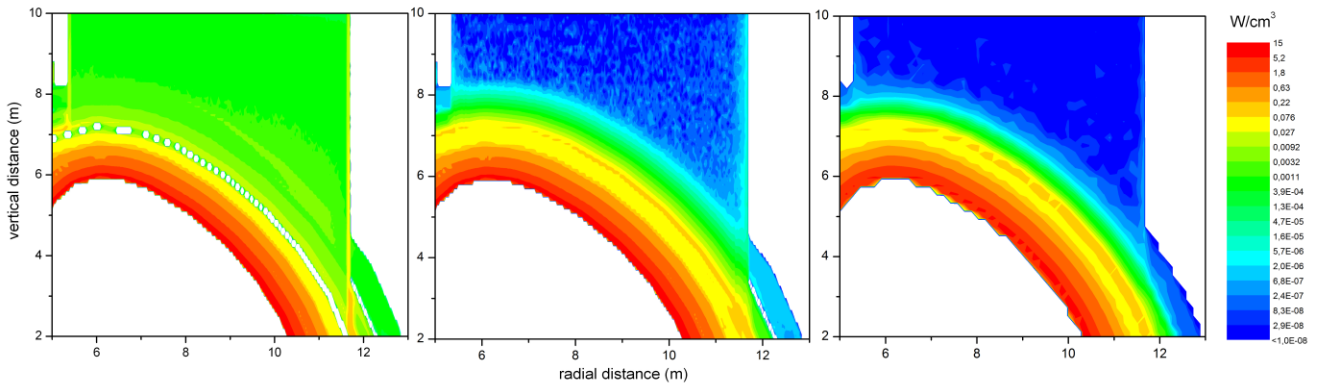
Figure 12. Comparison (in radial-poloidal sections) of the power density in the surrounding of the Upper Port between the unshielded Port of model 1 (left) and the two shielded Ports of model 5 (middle) and 6 (right).

The fact that the IB values around the equatorial plane (figure 10b) were still very near to the limit, and also considering that others limits - like the neutron fluences in the epoxy insulator and in the superconductor, the dpa in the copper stabiliser but also the helium production in the structural steel – used to be more restrictive [29], it was decided to improve the design of the Shield system.

4.3 Shield modifications. Resultant nuclear heating in winding pack.

It is well known that in tokamaks the available space in the inboard zone is limited for the presence of the central solenoid. Due to this reason is not possible to improve the shield efficiency of the IB zone simply enlarging the thickness of the components in this zone. Furthermore, considering: 1) that not only the TF coil but also the VV could be affected by the high radiation especially at the equatorial inboard level; and 2) the high TBR values achieved (1.22), it has been decided to improve the shielding capability looking at the Shield itself: reducing the thickness of the breeder zone in favour of the Shield thickness and testing different Shield materials with better neutron and/or gamma shielding performances.

To implement these modifications, the thickness of the outer LiPb channels has been reduced from 38 to 32 cm (reducing the whole breeder zone from 76 to 70 cm). The recovered 6 cm could now be considered as a separate component, the High Temperature Shield (HTS). Having two separate components could suppose an advantage when only the first centimeters of the whole shield system do not withstand the radiation. In fact, instead of removing the whole Shield (implying also a major waste problem), only the high temperature part would be substituted, while the other 30 cm of Shield would be maintained as Low Temperature Shield (LTS) operating during the whole life of the reactor. Nevertheless the inconvenient of an additional "locking system" should not be underestimated.

Different combinations of materials for the two Shielding systems have been tested according to table 7. In addition to Eurofer, other materials as WC and metal hydrides have been tested. The metal hydrides selected, TiH_2 and ZrH_2, combine the high moderation capabilities of fast neutrons (provided by the high hydrogen atoms density, higher than water) with the neutron absorption provided by Ti and Zr atoms. From the list of the metal hydrides potential candidates those which can prevent hydrogen release at less than 600 ºC have been chosen [31][32][35][34][36]. As it is possible to see in table 7, in which the new TBR results are also shown, the reduction of breeder zone has implied only a weak reduction of the TBR that continues to be above the self-sufficiency criterion (1.1). Finally, versions numbered n.1 and n.2 in table 7 (and so on in the text) use the two different shielded Ports described in section 4.2 while versions n.3 uses a more conventional mixture for the VV wall composition (without W).

The results of the power density in the TF-coil for all the previous versions (of table 6) and for the new combinations of Shield and VV materials (of table 7) are shown in figures 13a (inboard) and 13b (outboard). Comparing the last of the preceding options (cyan line) with the new Eurofer dimension (pink line) for both IB and OB sides no strong difference in the power density is observed. In fact LiPb and Eurofer (Li-6 and Fe) in certain energy domain (10^4-10^6eV) have similar neutron absorption cross-section values. Otherwise

comparing with the 6 cm WC option (purple line) there is a clear improvement of the result (C moderates thus the neutron absorption of W increase). Furthermore the use of a different Port (number 1or 2) make more pronounced this difference (in the OB side where the Port presence is relevant) repeating the same pattern for the different shielding combinations. Finally, the use of any combination with a metal hydride has a major impact on the nuclear heating at all TF-coil heights (because of the powerful moderator, H, that implies a higher exploitation of the neutron absorber, Ti/Zr).

Table 7. Summary of the configurations (materials and thicknesses) tested for the HT and LT Shields, in combination with different VV and Ports. In the last column the new TBR values are also shown.

model	HT Shield	LT Shield	VV walls	Upper Port	TBR
7.1	6 cm Eurofer	30 cm Eurofer	66.5% SS316LN 30% W 3.5% water	Shield_1	1.216
8.1	6 cm WC	" "	" "	Shield_1	1.202
8.2				Shield_2	
9.2	" "	30 cm TiH$_2$	" "	Shield_2	
10.1	" "	30 cm ZrH$_2$	" "	Shield_1	1.187
10.2			" "	Shield_2	
10.3	" "	" "	95.3% SS316LN 4.7% water	Shield_1	
8.3	" "	30 cm Eurofer	" "	Shield_1	
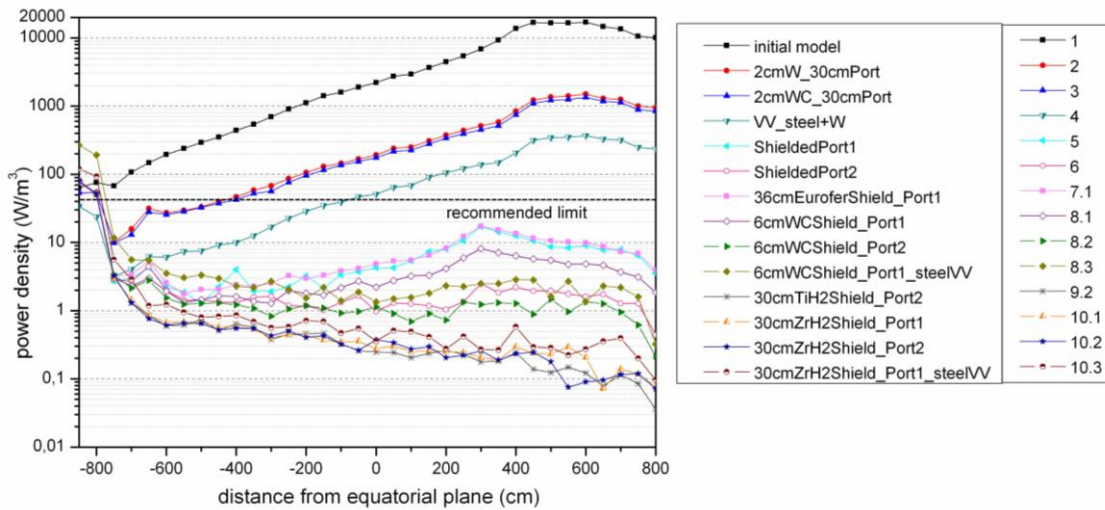
a)
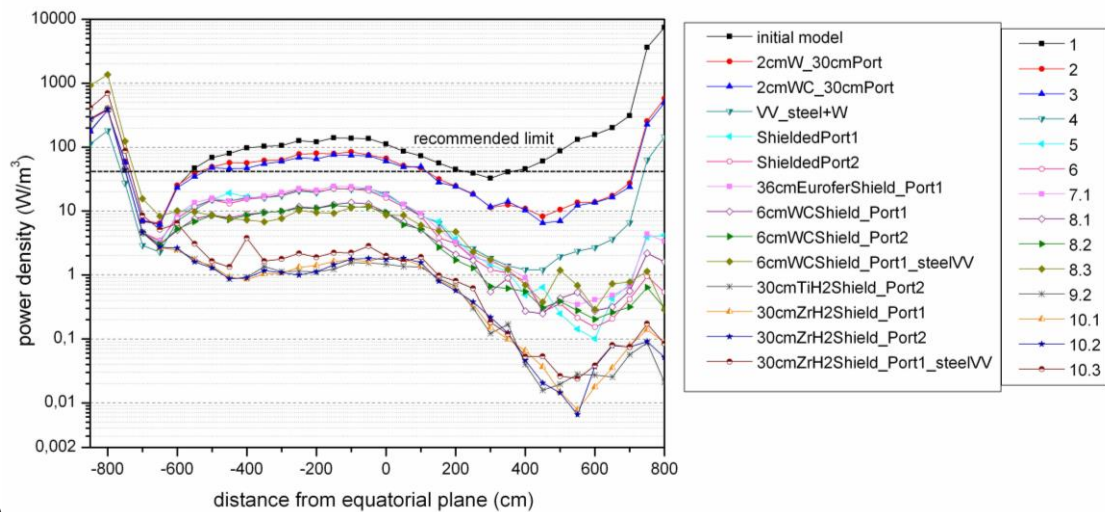
b)

Figure 13. Poloidal distribution of the power density (W/m^3) in the OB (a) and IB side (b) of the TF coil for the different configurations of the VV and Shield tested.

4.4 Radiation damage to the TF coil

In order to have a complete evaluation of the radiation effect on the TF-coil, together with the nuclear heating in the WP, the other neutronic responses from table 5 have also been studied for all the versions previously described of the *detailed* model. Both a DEMO and a Power Plant (PP) scenarios have been simulated, assuming for the first, the 20 years pulsed scenario (that at 30% of availability are equivalent to 6 full power years, FPY) of DEMO1 [37], a near-future technology, pulsed, version of DEMO, established in 2012 [38][39] in the frame of the new European Roadmap Horizon 2020 [40]; and for the second, a Commercial Power Plant scenario of 40 FPY.

4.4.1 Neutron fluence

Usually the peak of neutron fluence in the TF coil is found at the inboard mid-plane, but here, as the presence of the Upper Port and a not-optimized divertor made it difficult to establish the most irradiated point in each version (partially deductible from the pattern of the curves of figure 13), three responses have been calculated as global values in the whole TF coil:

1) Peak fast neutron fluence (E > 0.1 MeV) to the Nb_3Sn superconductor [cm^{-2}],
2) Integral neutron fluence for to the Nb_3Sn superconductor [cm^{-2}], and
3) Integral neutron fluence for epoxy insulator [cm^{-2}],

The values per year, for 6 FPY and for 40 FPY for the 3 parameters and for the 14 versions of the *detailed* model are listed in table 8.

Table 8. Results of neutron fluences in the winding pack and in the epoxy of the TF-coil for the 14 models developed, giving values per year, per 6 FPY and per 40 FPY. A colour scale has been created to define the goodness of the results as explained in the text.

Parameter:	fast neutron fluence in superconductor (WP)			integral neutron fluence in WP			integral neutron fluence in epoxy		
Design limit:	10^{18} cm^{-2}			*no established limit			10^{18} cm^{-2}		
MODEL	1/cm² year	*6FPY	*40FPY	1/cm² year	*6FPY	*40FPY	1/cm² year	*6FPY	*40FPY
1	4.61E+18	2.77E+19	1.84E+20	8.81E+18	5.29E+19	3.52E+20	1.34E+19	8.04E+19	5.35E+20
2	3.25E+17	1.95E+18	1.30E+19	6.72E+17	4.03E+18	2.69E+19	1.06E+18	6.36E+18	4.26E+19
3	2.87E+17	1.72E+18	1.15E+19	5.96E+17	3.58E+18	2.39E+19	9.48E+17	5.69E+18	3.79E+19
4	1.03E+17	6.18E+17	4.13E+18	2.10E+17	1.26E+18	8.39E+18	3.30E+17	1.98E+18	1.32E+19
5	4.85E+16	2.91E+17	1.94E+18	7.78E+16	4.67E+17	3.11E+18	1.04E+17	6.24E+17	4.15E+18
6	4.60E+16	2.76E+17	1.84E+18	7.24E+16	4.34E+17	2.90E+18	9.48E+16	5.69E+17	3.79E+18
7.1	5.07E+16	3.04E+17	2.03E+18	8.11E+16	4.87E+17	3.24E+18	1.08E+17	6.48E+17	4.32E+18
8.1	4.69E+16	2.81E+17	1.88E+18	7.37E+16	4.42E+17	2.95E+18	9.65E+16	5.79E+17	3.86E+18
8.2	4.52E+16	2.71E+17	1.81E+18	7.04E+16	4.22E+17	2.82E+18	9.12E+16	5.47E+17	3.65E+18
8.3	1.35E+17	8.10E+17	5.38E+18	2.02E+17	1.21E+18	8.08E+18	2.52E+17	1.51E+18	1.01E+19
9.2	4.35E+16	2.61E+17	1.74E+18	6.70E+16	4.02E+17	2.68E+18	8.60E+16	5.16E+17	3.44E+18
10.1	4.39E+16	2.63E+17	1.76E+18	6.77E+16	4.06E+17	2.71E+18	8.69E+16	5.21E+17	3.47E+18
10.2	4.35E+16	2.61E+17	1.74E+18	6.71E+16	4.03E+17	2.68E+18	8.60E+16	5.16E+17	3.44E+18
10.3	5.81E+16	3.49E+17	2.32E+18	9.08E+16	5.45E+17	3.63E+18	1.19E+17	7.14E+17	4.75E+18

According to table 8 in which a colour scale has been created to indicate the level of suitability of the achieved results, the values in red are those which exceed considerably the limits of table 5, then follow the *green*, the **blue** and the grey numbers. The **black** values are those which fulfils completely the limits. Considering these criteria, the models with white background 1, 2, 3, 4 and 8.3 would not be able to operate during 6 FPY nor 40 FPY. The other background colours indicate the models which satisfy the limits during a period of 6 FPY but not of 40 FPY although getting closer to fulfil them going from *green* (*7.1, 10.3*) to **blue** (*5, 6, 8.1, 8.2*) to **grey (9.2, 10.1, 10.2)**. For one of the model of the "*green* category" (the worst category of those which overcome the barrier of 6 FPY), model *10.3*, and one of "**grey** category" (the best), model **10.1**, both using a metal hydride as LTS, the spatial map distribution of the integral neutron fluence in the IB and OB mid-plane has been analysed. The results displayed in figure 14 (left: model 10.1, right: model 10.3, up:

IB equatorial plane, down: OB equatorial plane) show that, for both models 10.1 and 10.3, in the winding pack (that is the inner rectangle), in the epoxy (the intermediate rectangle) and for both IB and OB side, the limit of 10^{18} cm^{-2} is fulfilled also considering a period of 40 FPY, being the maximum 7.3×10^{17} cm^{-2}.
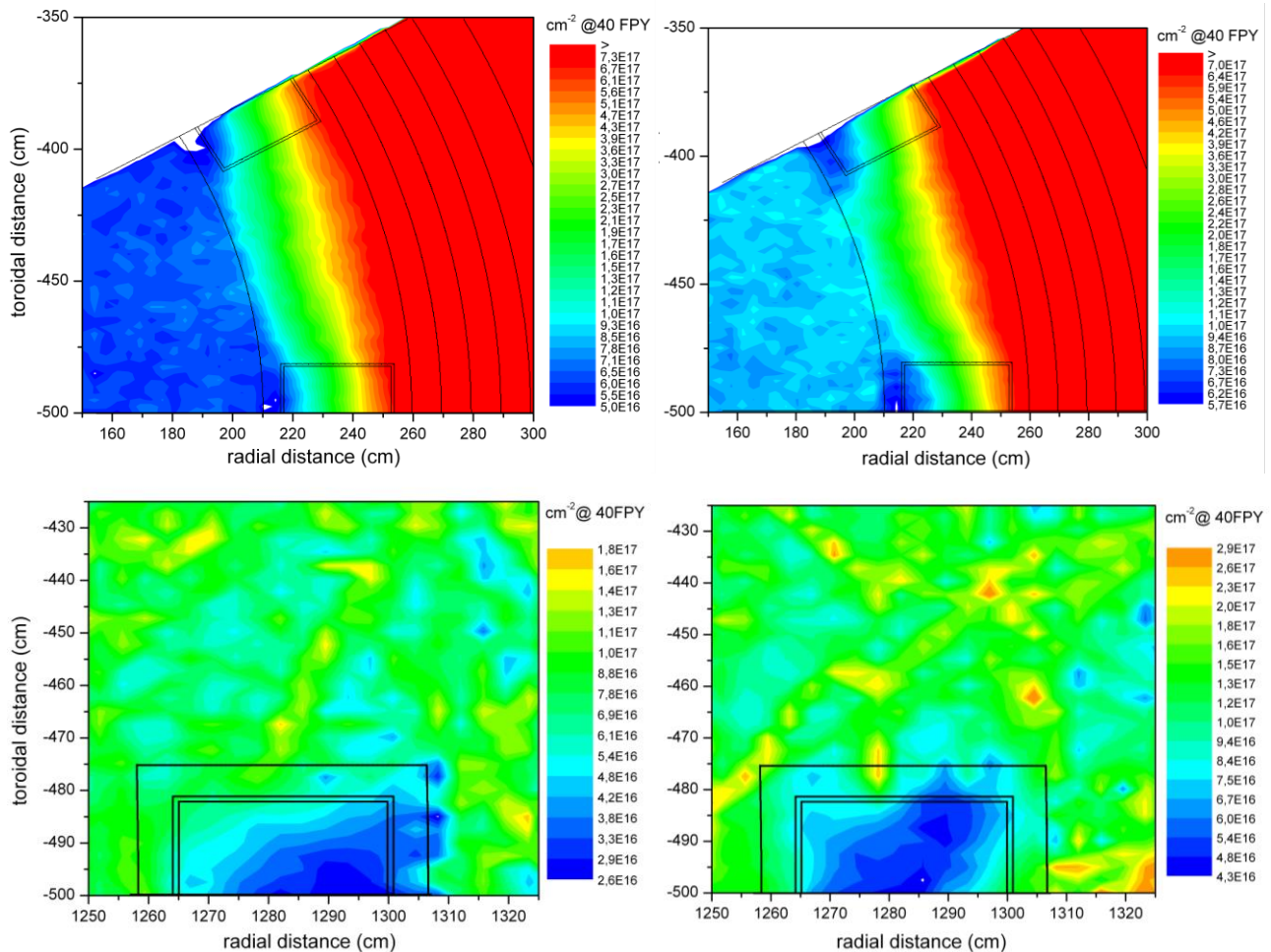
Figure 14. Results of neutron fluence to the TF-coil in radial-toroidal sections at the equatorial plane after 40 FPY (left: model 10.1, right: model 10.3, up: IB side, down: OB side).

This means that the global values of table 8 are higher than the local values at the mid-plane because the maximum is reached at the divertor level (that was not under development in this work) as could be deduced from the peaks of figure 13 at divertor heights (at -8 m high from the mid plane). The results for models 10.1 and 10.3 could be extrapolated to all the others models which belong to the three categories (green, blue and grey) because the behaviour of all the models from the nº 5 is the same, with the maximum of nuclear heating at divertor level. Thus, it might be deduced that they should respect the fluence limit at 40 FPY because the global values overestimate the punctual ones at all the others levels.

4.4.2 Peak displacement damage to the copper stabiliser

The last criteria that is needed to be observed to preserve the TF-coil from *quench* is the peak displacement damage to the copper stabiliser which limit has been established in 10^{-4} dpa (table 5). This has been calculated using the NRT method [41] within the MCNP code as explained by [42] through which the fluence rate and the displacement cross section MT 444 in the material (energy damage * 0.8/ threshold energy to displace the atom from the lattice, typically 40 eV) are used to calculate the damage in dpa terms. This parameter has been studied for (at least) one model for each of the above categories: model 1, 5, 8.3, 10.1 and 10.3, as shown in table 9.

Table 9. Displacement per atoms (dpa) per year and for 6 and 40 years of operation (*Full Power Years*) as global values in the copper stabilizer of the TF-coil for 5 versions of the *detailed* model.

model	damage to copper stabiliser		
	dpa/yr	*6FPY	*40FPY
<u>1</u>	4.94E-04	<u>2.96E-03</u>	<u>1.98E-02</u>
5	9.51E-06	**5.71E-05**	*3.80E-04*
<u>8.3</u>	3.27e-05	<u>1.96E-04</u>	<u>1.31e-03</u>
10.1	9.36e-06	**5.62E-05**	<u>3.74e-04</u>
10.3	1.21e-05	**7.26E-05**	*4.85e-04*

As noted in previous section 4.4.1, the models appear to repeat the same behaviour, being model 1 and 8.3 not suitable neither for DEMO nor for a PP, while models 5, 10.1 and 10.3 seem possible for being operated during 6 FPY, and from green (10.3) to blue (5) to grey (10.1) even closer to be operated during 40 FPY.

The peak values extrapolated from the spatial maps distributions and listed in table 10 show that model 5 has the maximum value (<u>red underlined</u>) in the IB mid-plane and can operate during 6 FPY while for models 10.1 and 10.3 the global values overestimate the punctual values in the regions of interest, resulting that model 10.3 could actually operate during more than 20 FPY (40 years at more than 50% availability) and model 10.1 is very near to be used as Power Plant during 40 FPY.

Table 10. Displacement per atoms (dpa) comparison between the global values and the peak values at the IB and OB equatorial plane of the TF-coil's copper stabilizer for 4 very different models.

model	Global value	Peak in OB mid-plane			Peak in IB mid-plane		
	dpa/yr	dpa/yr	*6FPY	*40FPY	dpa/yr	*6FPY	*40FPY
<u>1</u>	4.94E-04	<u>5.8E-4</u>	3.48E-03	2.32E-02	4E-5	2.40E-04	1.6E-3
5	9.51E-06	7E-7	**4.20E-06**	**2.80E-05**	<u>1.54E-5</u>	**9.24E-05**	*6.16E-04*
10.1	<u>9.36E-06</u>	3.36E-07	**2.02E-06**	**1.34E-05**	2.86E-06	**1.72E-05**	<u>1.14E-04</u>
10.3	<u>1.21E-05</u>	4.59E-07	**2.75E-06**	**1.84E-05**	4.46E-06	**2.68E-05**	*1.78E-04*

4.5 Radiation damage to the structures

Besides guaranteeing the superconductivity of the TF coils, indispensable to keep the plasma confinement, another essential requirement is to assure the structural integrity of the components. For this purpose, two different primary damage parameters that could indicate the suitability of the developed models have been analysed in the steel components: the helium production and the dpa. The reference limits adopted for these parameters are summarized as follows:
- According to [43] the helium production (appm He) in the steel components must be less than 1 appm at the end of life in order to allow re-welding
- The re-weldability limit for the austenitic steel could be increased up to 10 appm He [44]
- The ferritic steels could operate until 150-200 dpa [45] however the progressive start up for the new DEMO1 plans to use a "starter" blanket with 20 dpa damage limit in the first wall steel, and then switch to a second set of blankets with a 50 dpa damage limit [38]
- The irradiation damage limit proposed among the new EUROfusion activities [46] for the austenitic steel 316LN is 2.75 dpa, in agreement with the results of the irradiation tests performed for ITER [47][48].

4.5.1 Helium production
The helium production in terms of appm He per year has been calculated for all the previous described models in all the steel components that are supposed to be permanent: Low Temperature Shield (made of Eurofer), Vacuum Vessel walls and Port (made of austenitic steel or austenitic steel + tungsten). Results are shown in table 11.

Helium is produced typically in the absorption reactions (n,a) as the $^{10}B(n,a)^{7}Li$ reaction. Actually, the collision of neutrons on B^{10} produce helium trough the two reactions: 1) $B^{10} + n \rightarrow Li^{7}$ (0.84 MeV) + He^4 (1.47

MeV) + γ (0.48 MeV) (the 94% of the time); and 2) $B^{10} + n \rightarrow Li^7$ (1.02 MeV) + He^4 (1.78 MeV) (the 6% of the time). For this reason it has been preferred, as in [1], to use simple steel or tungsten + steel mixture in the walls of the VV and in the Port (instead of borated steel) even though borated water is employed in the zone between the two VV walls to take advantage of the absorption capability of the boron.

Assuming the conservative criterion of 1 appm He as maximum [43], the VV of all the models from version nº4 could be a permanent component for a DEMO reactor (6 FPY), according to the results of helium production (table 11). Models 1, 2, 3 and 7.1 have some components that fail the criterion of 1 appm He as maximum, even for a DEMO reactor. In particular, model 7.1 that enlarges the Eurofer Shield suffers from a deterioration of the rewelding capability of the LTS that seems not suitable to be a permanent component of a DEMO. Model 6 and 8.3 LTSs seem suitable for a DEMO reactor operating during 6 FPY. The lifetime of the models 4, 5, 8.1, 8.2 and 10.3 could be protracted until 20 FPY (40 years at 50% availability) substituting only the LTS after 6 FPY of operation. Model 10.3 have the advantage to use ZrH_2 as LTS, eliminating the problem of helium production in steel. In this way the LTS could be considered permanent under this criteria. Models 10.1 and 10.2 also uses ZrH_2 instead of Eurofer in the LTS, eliminating the problem of the helium production in this component. Furthermore, as it is possible to see, the values in the VV are so low that we can consider these versions as possibilities for a Power Plant operating during 40 FPY, also considering the results of the previous analyses.

Table 11. Helium production global values (in appm He) for 1 and 40 years of operation (*Full Power Years*) in the Low Temperature Shield of Eurofer and in the two walls of the Vacuum Vessel and in the Upper Port, for most of the models previously developed.

model	LTS		Inner wall of VV		Outer wall of VV		Upper Port	
	appm He/yr	*40FPY	appm He/yr	*40FPY	appm He/yr	*40FPY	appm He/yr	*40FPY
1	0.191	7.633	0.475	18.985	0.01	**0.394**	0.107	4.267
2	0.146	*5.820*	0.300	11.994	0.002	**0.075**	0.094	3.755
3	0.146	*5.837*	0.291	11.644	0.002	**0.069**	0.090	3.581
4	0.142	*5.674*	0.049	*1.962*	0.0003	**0.012**	0.007	**0.297**
5	0.142	*5.697*	0.055	*2.195*	0.001	**0.027**	0.003	**0.126**
6	0.142	*5.681*	0.048	*4.952*	0.0005	**0.019**	0.002	**0.061**
7.1	0.194	7.762	0.041	*1.658*	0.0005	**0.019**	0.002	**0.099**
8.1	0.122	*4.874*	0.046	*1.855*	0.001	**0.027**	0.002	**0.090**
8.2	0.122	*4.884*	0.038	*1.513*	0.0005	**0.018**	0.001	**0.041**
8.3	0.063	*2.523*	0.141	*5.649*	0.004	**0.164**	0.001	**0.057**
10.1	-	-	0.015	**0.596**	0.00043	**0.017**	0.00003	**0.001**
10.2	-	-	0.014	**0.548**	0.00034	**0.013**	0.00002	**0.00093**
10.3	-	-	0.053	*2.128*	0.00085	**0.034**	0.00004	**0.002**

According to the detailed distributions maps obtained through the "mesh tallies" capabilities of MCNP for models 5, 8.1 10.1 and 10.3, the peak values in the IB equatorial plane for model 5 and 8.1 are higher than the global values of table 11, being 0.4 appm He/yr in Shield (while the global values are 0.12-0.14 appm He/yr), and 0.09-0.08 appm He/yr in the inner wall of the VV (while the global values are around 0.05 appm He/yr). On the contrary, for model 10.1 the peak equatorial values in the inner wall of the VV are lower than the global value (of 0.015 appm He/yr) being 0.004 appm He/yr in the IB and 0.008 appm He/yr in the OB side. For model 10.3, similarly but in a less pronounced way, the IB value at the mid-plane is 0.05 appm He/yr and the OB value is 0.008 appm He/yr lesser than the 0.053 appm He/yr global value. These results entail that the forecast of operation during 40 and 20 FPY is correct for models 10.1 and 10.3, respectively, while the outlook for models 5 and 8.1 needs to be adjusted to the local values of the maps, resulting the VV of these models feasible during 10 FPY and the LTS during 3 FPY with a strong implication on the concept of Shield system that in this case should be a removable piece together with the BB system. The conclusions on the VV lifetime would relax if the 10 appm He limit [44] is further demonstrated.

4.5.2 Displacement damage and helium/dpa ratios
The helium production and the displacement damage have been evaluated as global values in the First Wall of the reactor (being the same for all the models) giving results for 1, 5 and 10 full power years of operation. The results are shown in table 12. The ratios helium/dpa are also given.

Table 12. Helium production (in appm He) and displacement per atoms (in dpa) global values for 1, 5 and 10 years of operation (*Full Power Years*) and He/dpa ratios, in the Eurofer First Wall of the two IB and OB equatorial modules.

First Wall	appm He			dpa			He/dpa
	1FPY	*5FPY	*10FPY	1FPY	*5FPY	*10FPY	
OB	110.53	552.66	1105.3	14	70	140	7.89
IB	73.71	368.53	737.1	10.4	52	104	7.08

Assuming the limit of 150 dpa [45], the structural material (Eurofer) of the First Wall could have a lifetime of more than 10 years, that would improve the result of an older study on a *simplified* version of our model [49][49] that showed a service life around 6 years. Considering the values in the equatorial plane at the IB and OB sides extrapolated from the "mesh tally" calculated in Eurofer, the local values for both He and dpa result higher than the global values of table 12, being 180/270 appm He year^{-1} and 18/27 dpa year^{-1} for the IB/OB side, and being 10 the ratio He dpa^{-1} in both the two cases. If 18/27 dpa year^{-1} are assumed as maximum values, the service life for the blanket modules will be of 8.3/5.5 FPY (IB/OB) taking into account the limit of 150 dpa. For a Power Plant scenario, this means ~ 4/7 replacements during the 40 FPY of operation. For DEMO1, as more conservative criteria of 20 + 50 dpa have been assumed [39] driving the scheduled maintenance programme [38], the "starter" modules should be substituted at 1.1/0.74 FPY (IB/OB), and the second set of modules after 2.7/1.8 FPY (IB/OB), meaning that these OB modules should be replaced twice during the 6 FPY of operation of the reactor.

Finally, the global values of dpa and helium/dpa ratios in Eurofer LTS and in Austenitic steel VV have also been assessed giving results in table 13. The austenitic steel used in the VV walls is the cause of higher helium/dpa ratios than the obtained in the Eurofer components. Relatively lower values are obtained when tungsten is added to the austenitic steel VV walls (model 5 and 10.1). In fact the helium production in W is usually 10 times lesser than in Fe (while dpa values are similar in Fe and W) [50] [51]. The dpa limits are fully met for LTS and both VV walls, being the accumulated values after 40 years full operation (PP scenario) less than 150 dpa (limit for Eurofer) [45] and 2.75 dpa (limit for Austenitic steel 316LN) [46].

Table 13. Damage in dpa (per year, and for 40 *Full Power Years*) and ratios helium/dpa in the steel of the LTS and VV walls for some of the versions studied.

model	LTS			Inner wall of VV			Outer wall of VV		
	dpa/yr	*40FPY	He/dpa	dpa/yr	*40FPY	He/dpa	dpa/yr	*40FPY	He/dpa
1	0.152	6.10	0.79	4.67E-02	1.87	10.2	6.22E-04	2.49E-02	16.08
5	0.158	6.32	1.11	3.54e-02	1.42	1.55	8.54E-05	3.42E-03	11.71
8.3	0.0168	0.672	0.26	1.66e-02	0.66	8.49	3.47e-04	1.39E-02	11.53
10.1	-	-		1.13e-02	0.45	1.33	8.19e-05	3.27e-03	5.25
10.3	-	-		1.16e-02	0.46	4.57	1e-04	4e-03	8.50

5. Conclusions

Based on the plasma parameters of the PPCS model C and starting from the radial build determined in a *simplified* version of a DCLL model in which the real structures were substituted by homogenized equivalent layers, a *detailed* 3D preliminary design has been produced keeping all the neutronic relevant details with the corresponding heterogeneous compositions. The neutronic design has been developed by means of a specifically developed software which approximates the curved profiles of the CAD model to the union of segments within a given tolerance. After that, the STEP model can be converted to the geometric input of the Monte Carlo code MCNPX using the conversion programme MCAM and then the transport analysis with MCNPX is performed to predict the main neutronic responses of the design.

The initial model has been then optimized according to the neutronic results, looking to achieve the basic capabilities required for a fusion reactor: tritium production, energy multiplication, shielding of the TF-coil to maintain the plasma confinement and shielding of the structural component to keep their integrity. Materials and thicknesses for the Shield and the VV's walls and Port have been modified to limit the radiation effects on the TF coils as well as to guarantee the lifetime protection of the steel components.

Hence, different versions of the *detailed* 3D model for a DCLL DEMO/PP have been developed. According to the analyses performed on them, the better behaviour under the simulated radiation has been obtained for the configurations labelled 9.2, 10.1 and 10.2 that use metal hydrides in the Low Temperature Shield, tungsten carbide in the Hot Temperature Shield, and that have a Vacuum Vessel employing a mixed composition with tungsten. Even though these materials are more expensive and advanced than the actual state of technology, they should allow the operation of the reactor during 40 FPY (at 100% availability), thus meaning that they could be the option for a future Commercial Power Plant (on the condition of providing a slight improvement for the shield of the copper stabiliser TF-coil whose damage has resulted slightly higher than the recommended limit).

For a demonstration plant DEMO - that according to the last European approach, more pragmatic than the previous one, should operate in a pulsed regime and should be based on existing technologies - several of the options presented in this paper, from nº 5 to 10.3, would be suitable allowing an efficient operation of the reactor during a period of 6 FPY. Some are more conservative, like the nº 5 that uses a single Shield of Eurofer, and others, more audacious, like the nº 8.1 that replace part of the Eurofer with tungsten carbide for the HTS, or the nº 10.3 that, additionally, uses zirconium hydride for the LTS. This option does not have tungsten in the Vacuum Vessel which therefore would be easier to build (steel and water only). According to the results presented in the previous section, this option could also be adopted for a 40 years power plant but with lower availability (at 50% that are 20 FPY). The results have also shown the need of an horizontal shield inside the Upper Port of the Vacuum Vessel, resulting enough a steel and water shield for both the scenarios: DEMO and Commercial Power Plant.

The high value of TBR obtained for the first version of the *detailed* model (1.23 with 90% enrichment in Li-6) has allowed reducing the breeder region in favour of the improvement of the shielding capabilities provided by the Shield itself. In a first attempt to do it, a reduction of the outer breeder channels from 38 to 32 cm (total breeder zone from 76 to 70 cm) and the consequent increase of the Shield thickness from 30 to 36 cm have implied a reduction of the TBR to 1.22-1.19 (depending on the Shielding material behind the blanket). Thus, a TBR still enough to guarantee the fuel sustainability of the reactor has been achieved for all the considered models.

The shielding of the reactor could have been also improved by increasing more the Shield thickness at the expense of the breeder zone thickness, thanks to the still high performances of tritium production of this one. However, it seemed better to be conservative and consider a significant breeder margin in order to allow a potential reduction of the Li-6 enrichment. In fact, even with 50% Li-6 enrichment the TBR would be around 1.14 being still above the limit for fuel self-sufficiency. Furthermore, the design could be the basis for a modular DCLL blanket model in which more structural material should be required with a consequent TBR reduction.

At this purpose, it should be emphasized that the poloidal distributions of the nuclear responses previously analysed are very useful to convert the banana-shape blanket design, here adopted, in a modular blanket design in which each module could have a different thickness according to the efficiency of power recovery and tritium production of each corresponding poloidal zone. In fact, some of the results here presented are being the basis for the newly established European program activities EUROfusion for the next 4 years, in which they are helping to design a pulsed DEMO with DCLL modular breeding blanket.

Acknowledgments

References

[1] Palermo I *et al*, Neutronic design analyses for a dual-coolant blanket concept: Optimization for a fusion reactor DEMO, *Fus. Eng. Des.* 87 (2012) 1019–1024.

[2] Malang S *et al*, Dual Coolant Blanket Concept, Kernforschungszentrum Karlsruhe, *KfK 5424*, November 1994.

[3] Tillack M S *et al*, High Performance PbLi blanket, *Proceedings of the 17th IEEE/NPSS Symposium on Fusion Engineering*, San Diego CA, October 1997.

[4] Norajitra P *et al*, Conceptual Design of the Dual-Coolant Blanket within the Framework of the EU Power Plant Conceptual Study (TW2-TRP-PPCS12), Forschungszentrum Karlsruhe GmbH, Karlsruhe, *FZKA 6780*, 2003.

[5] Li J, Wu Y, Zheng S, Preliminary neutronics design of the dual-cooled lithium lead blanket for FDS-II, *Proceedings of the 23rd Symposium on Fusion Technology*, Venice, Italy, Sep. 20-24, 2004.

[6] Wang H *et al*, Preliminary thermal hydraulics design of the dual-cooled lithium lead blanket for FDS-II, *Proceedings of the 23rd Symposium on Fusion Technology*, Venice, Italy, Sep. 20-24, 2004.

[7] Raffray A R *et al*, Engineering Design and Analysis of the ARIES-CS Power Plant, *Fusion Science and Technology* 54 (3), Pages 725-746, 2008.

[8] Wong C P C *et al*, An overview of dual coolant Pb-17 Li breeder first wall and blanket concept development for the US ITER-TBM design, *Fus. Eng. Des.* 81, 461-67, 2006.

[9] Wong C P C *et al*, An overview of the US DCLL ITER-TBM program, *Fus. Eng. Des.* 85, Issues 7-9, 1129-32, December 2010.

[10] Wu Y and the FDS Team, Design status and development strategy of China liquid lithium-lead blankets and related material technology, *J. Nucl. Mater.* 367-370, 1410-1415, 2007.

[11] Wu Y and the FDS Team, Overview of Liquid Lithium Lead Breeder Blanket Program in China, Fusion Engineering and Design, *Fus. Eng. Des.*, 86, Issues 9–11, 2343-46, October 2011.

[12] Malang S *et al*, Development of the Lead Lithium (DCLL) Blanket Concept, *Fusion Science And Technology* Vol. 60 July 2011.

[13] Maisonnier D *et al*, EFDA, A conceptual study of commercial fusion power plants, Final report of the European fusion power plant conceptual study (PPCS), *EFDA-RP-RE-5.0*, 2005.

[14] Maisonnier D *et al*, Power plant conceptual studies in Europe, *Nucl. Fusion* 47 (2007) 1524–32.

[15] Juanas J, Fernández I, Diseño de componentes internos y externos del Programa Consolider TECNO FUS, Technical Report, EURATOM-CIEMAT Association, Ref: CSD2008-079, 2009.

[16] Ibarra A, Veredas G, Fernández I, CIEMAT DCLL design, 1st EU–US DCLL Workshop, Karlsruhe, April 23-24th 2013.

[17] Li J *et al*, Comparison analysis of 1D/2D/3D neutronics modeling for a fusion reactor, *Fus. Eng. Des.* 83 (2008) 1678-1682.

[18] Sawan M E, Youssef M Z, Three-dimensional neutronics assessment of dual coolant molten salt blankets with comparison to one-dimensional results *Fus. Eng. Des.* 81 (2006) 505–511

[19] Wu Y, FDS Team, CAD-based interface programs for fusion neutron transport simulation, *Fus. Eng. Des.* 84 (2009) 1987-1992.

[20] Pelowitz D B (ed.), MCNPX User's Manual Version 2.6, Report LA-CP-07-1473 (2008).

[21] Petrizzi L *et al*, Helium-cooled lithium lead: Activation analysis of the test blanket module in ITER, *Fus. Eng. Des.* 83 (2008) 1244–1248

[22] Hubberstey P *et al*, Is Pb-17Li really the eutectic alloy? A redetermination of the lead-rich section of the Pb-Li phase diagram (0.0 <xLi (at%) < 22.1), *Journal of Nuclear Materials* 191-194, 283-287, 1992.

[23] Sukegawa A M *et al*, Safety design of radiation shielding for JT-60SA, *Fus. Eng. Des.* 82, 2799–2804, 2007.

[24] Villari R *et al*, Neutronic analysis of the JT-60SA toroidal magnets, *Fus. Eng. Des.* 84, 1947-52, 2009.

[25] Fischer U *et al*, Neutronics requirements for a DEMO fusion power plant, Fusion Eng. Des. (2015), http://dx.doi.org/10.1016/j.fusengdes.2015.02.029

[26] Palermo I, Gómez Ros J M , Simulación con MCNPX del término fuente para la emisión neutrónica

del plasma, CONSOLIDER-TN-T01-CN-SIMNEU-001, ISBN: 978-84-7834-643-1, 2010.

[27]   Chadwick M B *et al*, ENDF/B-VII.0: next generation evaluated nuclear data library for nuclear science and technology, Nuclear Data Sheets 107 (2006) 2931–3060.

[28]   White M C, Photoatomic Data Library MCPLIB04: A New Photoatomic Library Based On Data From ENDF/B-VI Release 8, LANL internal memorandum X-5:MCW-02-111 and LA-UR-03-1019, 2002.

[29]   Fischer U *et al*, Neutronics design analyses of fusion power reactors based on a novel integral approach, *Fus. Eng. Des.* 84 (2009) 323-328.

[30]   Duchateau J L *et al*, Conceptual design for the superconducting magnet system of a pulsed DEMO reactor, *Fus. Eng. Des.* 88, 1609– 1612, 2013.

[31]   Chen Y *et al*, The EU Power Plant Conceptual Study—Neutronic Design Analyses for Near Term and Advanced Reactor Models, *FZKA 6763*, Forschungszentrum Karlsruhe, 2003.

[32]   Catalán J P *et al*, Neutronic assessment of candidate materials for TF coils shielding in a demo fusion reactor based on a DCLL blanket, *Fusion Science and Technology* Vol. 62 190-195, 2012.

[33]   Mota F, Palermo I, Gomez-Ros JM, Report for TA WP12-DTM-04-T10: Neutronic study to shield the upper vertical port of DEMO, *EFDA_D_2D5TAJ*, 2013.

[34]   Fernández I, Rosa E V, Palermo I, Development of a brazing connector for DEMO in-vessel components, *Fus. Eng. Des.* 89, 2363–67, 2014

[35]   Hayashi T *et al*, Neutronics Assessment of Advanced Shield Materials Using Metal Hydrides and Borohydrides for Fusion Reactors, *Fus. Eng. Des.* 81, 1285, 2006.

[36]   Hayashi T *et al*, Advanced Neutron Shielding Material Using Zirconium Borohydride and Zirconium Hydride, *J. Nucl. Mater.*, 386–388, 119, 2009.

[37]   Kemp R, WP11-SYS-01-ACT5, DEMO DESIGN SUMMARY: Summary parameters for DEMO1 and DEMO2 designs, *EFDA_D_2L2F7V* v1.0, 24 May 2012.

[38]   Harman J, DEMO Fusion Power Plant, Plant Requirements Document (PRD), *EFDA_D_2MG7RD*, 2014 and WP12 DEMO Operational Concept Description, *EFDA_2LCY7A,* 2012

[39]   Federici G *et al*, Overview of EU DEMO design and R&D activities, *Fus. Eng. Des.* 89, Issues 7–8, 882–889, 2014.

[40]   Romanelli F, Roadmap to the Realization of Fusion Energy, 2014, to appear in *Fus. Eng. Design* and http://www.efda.org/wpcms/wp-content/uploads/2013/01/JG12.356-web.pdf, November 2012

[41]   Norgett M J, Robinson M T, Torrens I M, A proposed Method of calculating displacement dose rates, *Nuclear Engineering and Design* 33, 50, 1975.

[42]   Hogenbirk A, An easy way to perform a radiation damage calculation in a complicated geometry, *Fus. Eng. Des.* 83, 1828-31, 2008.

[43]   Aymar R *et al*, The ITER design, *Plasma Phys. Control. Fusion*, 44 519, 2002.

[44]   Tsuchiya K *et al*, Re-weldability tests of irradiated austenitic stainless steel by a TIG welding method, *Journal of Nuclear Materials* 283-87 1210-1214, 2000.

[45]   Bloom E E *et al*, Materials to deliver the promise of fusion power – progress and challenges, *Journal of Nuclear Materials* 329–333, 2004.

[46]   Bachmann C, *EFDA_D_2MJZ8S v1.0* -Vessel dose limit definition, 2014

[47]   Van Osch E V *et al*, Irradiation testing of 316L(N)-IG austenitic stainless steel for ITER, *Journal of Nuclear Materials* 258-263 (1998) 301-307

[48]   Lind A, Bergenlid U, Mechanical properties of hot isostatic pressed type 316LN steel after irradiation to 2.5 dpa, *Fus. Eng. Des.* 58–59 (2001) 713–717

[49]   Catalán J P *et al*, Neutronic analysis of a dual He/LiPb coolant breeding blanket for DEMO, *Fus. Eng. Des.* 86, 2293–2296, 2011

[50]   Gilbert M R *et al*, An integrated model for materials in a fusion power plant: transmutation, gas production, and helium embrittlement under neutron irradiation, 2012 *Nucl. Fusion* 52 083019

[51]   Gilbert M R *et al*, Neutron-induced dpa, transmutations, gas production, and helium embrittlement of fusion materials, *Journal of Nuclear Materials* 442 (2013) S755–S760